Proc. Natl. Acad. Sci. USA
Vol. 87, pp. 9503–9507, December 1990
Biophysics

Electrostatic field around cytochrome *c*: Theory and energy transfer experiment

(fluorescence/molecular dynamics/protein/bimolecular rate/Poisson–Boltzmann equation)

SCOTT H. NORTHRUP*, THEODORE G. WENSEL†‡, CLAUDE F. MEARES†, JOHN J. WENDOLOSKI§, AND JAMES B. MATTHEW§¶‖

*Chemistry Department, Tennessee Technological University, Cookeville, TN 38505; †Chemistry Department, University of California, Davis, CA 95616; and §E. I. du Pont de Nemours Company, Central Research and Development Department, Wilmington, DE 19898

Communicated by Frederic M. Richards, August 20, 1990

ABSTRACT **Energy transfer in the "rapid diffusion" limit from electronically excited terbium(III) chelates in three different charge states to horse heart ferricytochrome *c* was measured as a function of ionic strength. Theoretical rate constants calculated by numerical integration of the Forster integral (containing the Poisson–Boltzmann-generated protein electrostatic potential) were compared with the experimental data to evaluate the accuracy of protein electrostatic field calculations at the protein/solvent interface. Two dielectric formalisms were used: a simple coulombic/Debye–Hückel procedure and a finite difference method [Warwicker, J. & Watson, H. C. (1982) *J. Mol. Biol.* 157, 671–679] that accounts for the low-dielectric protein interior and the irregular protein/solvent boundary. Good agreement with experiment was obtained and the ionic-strength dependence of the reaction was successfully reproduced. The sensitivity of theoretical rate constants to the choices of effective donor sphere size and the energy transfer distance criterion was analyzed. Electrostatic potential and rate-constant calculations were carried out on sets of structures collected along two molecular dynamics trajectories of cytochrome *c*. Protein conformational fluctuations were shown to produce large variations in the calculated energy transfer rate constant. We conclude that protein fluctuations and the resulting transient structures can play significant roles in biological or catalytic activities that are not apparent from examination of a static structure. For calculating protein electrostatics, large-scale low-frequency conformational fluctuations, such as charged side-chain reorientation, are established to be as important as the computational method for incorporating dielectric boundary effects.**

Electrostatic interactions are known to play a significant role in the biological activity of proteins, as indicated by the pH and ionic-strength dependence of virtually all protein reactions (1). Numerous studies have shown that reaction rates between proteins and charged substrates often depend strongly on the solution ionic strength. These observations have been taken to suggest that intermolecular electrostatic forces are important in facilitating the association of reaction complexes. To analyze specific interactions at the molecular level an accurate description of the electrostatic forces around the protein is essential. The electrostatic analysis of proteins by theoretical frameworks is usually couched in terms of the net charge and the dipole moment (2, 3), higher moments (4), or the full asymmetric charge distribution of a single structure derived by crystallography (5–10). One of the more rigorous approaches to the computation of the electrostatic field surrounding proteins in aqueous electrolyte solution involves the iteration of the Poisson–Boltzmann equation by the Warwicker–Watson (WW) algorithm (11). Starting with the protein crystal structure, this procedure accounts for (*i*) the irregular topography of the protein surface, (*ii*) the presence of diffusible ions in the medium, and (*iii*) the discontinuity in the dielectric constant and ionic strength across the protein/solvent boundary. This method has been useful in understanding the propagation of electric fields across irregular dielectric boundaries. Dielectric continuum models applied to a single structure do account for the effects of small-scale high-frequency fluctuation of protein structure through the effective dielectric constant; however, they do not account for large-scale conformational variability due to slower charged side-chain reorientation. Another fundamental question concerns refining computational methods based on an ensemble average structure (12) while experiments may represent the properties of a regularly occurring transient conformer. Here we examine how large-scale, slow, conformational fluctuations affect pH- and ionic strength-dependent predictions, and establish a protocol for determining the rms deviation for a computed value that is attributable to an average structure assumption.

Diffusion-enhanced energy transfer studies provide a convenient way to probe the electrostatic field surrounding proteins and DNA in solution (13). Accurate experimental energy transfer rates for charged probe behavior around charged macromolecules allow us to evaluate the accuracy of theoretical electrostatic methods. Experimental energy transfer rates from electronically excited terbium chelates to the heme of horse heart ferricytochrome *c* were measured (14) as a function of sodium chloride concentration for terbium probes in three different charged states: −1e, 0e, and +1e. Series of structures collected along molecular dynamics (MD) trajectories of horse heart cytochrome *c* were used to evaluate the sensitivity of electrostatic calculations and the predicted energy transfer rate constants to protein structural flexibility. Two different electrostatic computational formalisms were applied to these structures, a simple Debye–Hückel (DH) procedure and the WW finite difference method (11).

The second-order rate constant for dipole–dipole energy transfer in the rapid diffusion limit (i.e., diffusion is sufficiently rapid to provide an equilibrium spatial distribution of donors around acceptors) is obtained for a single structure by integrating the energy transfer rate (15) over all donor-

The publication costs of this article were defrayed in part by page charge payment. This article must therefore be hereby marked "*advertisement*" in accordance with 18 U.S.C. §1734 solely to indicate this fact.

Abbreviations: MD, molecular dynamics; WW, Warwicker–Watson; DH, Debye–Hückel; D80, MD trajectory with high dielectric formalism; DW, trajectory with explicit water molecules.

‡Present address: Baylor College of Medicine, Houston, TX 77030.
¶Present address: ICI Pharmaceuticals Group, Structural Chemistry, Wilmington, DE 19897.
‖To whom reprint requests should be addressed at present address.

acceptor geometries. The predicted bimolecular rate constant for energy transfer is then given by the volume integral:

$$k = 0.6023(R_o^6/\tau_o) \int\int\int dr\, r_{et}^{-6} e^{-\beta w(r)}\ M^{-1}sec^{-1}. \quad [1]$$

Here, R_o is the distance (nm) at which energy transfer is 50% efficient (16), and may be calculated from the measured properties of the donor emission and the acceptor absorption spectra as described elsewhere. The quantity τ_o is the excited-state lifetime (sec) in the absence of acceptor, and r_{et} is the distance (nm) from the donor to the acceptor. The electrostatic potential about the protein enters the problem through the equilibrium spatial weighting factor $e^{-\beta w(r)}$ containing the electrostatic potential energy $w(r)$ of the donor in the field of the protein. The quantity $\beta = (k_B T)^{-1}$, where k_B is the Boltzmann constant and T is absolute temperature. The substitution of the donor potential of mean force by the electrostatic potential of a single protein conformation assumes that the spatial relaxation of the donor is fast compared with the protein conformational fluctuation. Eq. 1 provides a theoretical means of calculating the rate constant when a knowledge of the conformation and electrostatic field of the protein is available. Analytical solutions to this integral have been reported where simple spherical models of the protein and donor are assumed (14). Here we apply the rigor of current numerical techniques, taking advantage of a detailed knowledge of the protein atomic coordinates. No attempt has been made to evaluate alternative mechanisms, such as exchange, to the energy transfer rates.

METHODS

Experimental. The Tb(III) chelates were $TbEDTA^-$ [terbium(III)–ethylenediaminetetraacetate], TbHED3A [terbium(III)–*N*-(2-hydroxyethyl)ethylenediaminetriacetate], and $TbBED2A^+$ [terbium(III)–*N*,*N*′-bis(2-hydroxyethyl)-ethylenediaminediacetate]. Horse heart cytochrome *c* was obtained from Sigma (type III). The commercial preparation contained various amounts of deamidated and aggregated forms in addition to the native protein (17) and about 20% of the reduced form. To obtain homogeneous, native ferricytochrome *c*, the commercial preparation was mixed with $K_3Fe(CN)_6$ and chromatographed on carboxymethyl cellulose with a sodium phosphate gradient according to Brautigan *et al.* (17). The details of the chromatographic procedure are given elsewhere (14).

Phosphate was removed by dialysis for several days against 0.1 M NaCl before addition of Tb(III) chelates (18). Extensive dialysis against distilled water reduced the NaCl concentration to below 1 mM. The deionized protein was stored as a frozen solution. The energy transfer distance R_o (Eq. 1) was calculated from the spectrum of the purified oxidized protein (14, 16), and found to be 3.7 nm with TbHED3A as energy donor. The rate constant for energy transfer to the heme from each donor chelate was determined at each salt concentration from the Tb(III) luminescence lifetimes in the presence and absence of cytochrome *c* (13). Over the range of experimental conditions, each luminescence decay was accurately fit by a single exponential (correlation coefficient, >0.99), indicating that all the donors were in equivalent average environments. This implies that protein binding of the chelates was not significant in these experiments.

To accurately measure the ionic-strength dependence of energy transfer to cytochrome *c*, samples were prepared with precisely determined NaCl concentrations. Large volumes (4–12.5 ml) of low-salt stock solutions were prepared, containing 50–100 μM cytochrome *c* and 0.2–0.4 mM Tb(III) chelate (either TbBED2A AcO, TbHED3A, or NH_4 TbEDTA). High-salt solution (0.1 M NaCl) was prepared with all the components except NaCl in the same concentration as in the low-salt stock. The two solutions were matched to give identical A_{490} values by addition of small (≈1 μl) aliquots of cytochrome *c* stock. A 1-μl aliquot of $^{22}NaCl$ (carrier-free) solution was added to each high-salt solution. This solution, of known NaCl concentration and measurable ^{22}Na specific activity, was used for all subsequent salt additions. The samples were made by addition of increasing amounts of high-salt solution to the low-salt stock. After each high-salt addition, duplicate aliquots were placed in 500-μl snap-cap Eppendorf vials for energy transfer measurements. Energy transfer experiments were performed immediately. Aliquots were weighed on an analytical balance and counted in the γ counter to determine the salt concentration. This procedure gave very precise measurements of the salt dependence of energy transfer (see Fig. 2). Experimental errors for the measured lifetimes, given in Table 3, are based on the variations between identically prepared samples and the uncertainty in the measured lifetimes. Larger errors for the neutral and positive terbium probes are due to lower accuracy in determining their shorter fluorescent lifetimes.

Computational. To study the effects of protein conformational variability on computed energy transfer rates, sets of protein conformers were collected at points along MD trajectories of horse heart cytochrome *c*, following the procedure reported for tuna cytochrome *c* (19). The initial coordinates for the horse species were prepared by amino acid substitution into the tuna crystallographic coordinates in a manner previously described (7). MD simulations were carried out on horse cytochrome *c* by using the program AMBER (version 2.0) coupled to GEMM (20) on an ST100 array processor. Trajectories were computed and an ensemble of structures was accumulated for two different dielectric constants (ε) in the AMBER nonbonded electrostatic energy term: $E_{ij} = Q_i Q_j / \varepsilon R_{ij}$. Here, R_{ij} is the charge-site separation between centers i and j and Q_i is the charge on center i. Following Wendoloski and Matthew (19), the dielectric formalisms were a high-dielectric model with $\varepsilon = 80$ and no explicit water molecules (D80 model) and a simulation where $\varepsilon = 1$ with 800 explicit TIP3P water molecules (21) included (DW model). These two different solvent-simulating dielectric treatments have been shown to give trajectory structures for cytochrome *c* that correspond well with the x-ray structure based on a variety of criteria: average atomic position (rms), ion pairs, solvent-accessible surface, and molecular volumes (19). The computations were carried out with a femtosecond time step and a coordinate set was saved every 50 fsec. The simulations were run for 150 psec (post-equilibration). Structures taken at 5-psec intervals from these trajectories were analyzed to determine the energy transfer rate constant. The extent of the side-chain reorientation between these structures and the resulting electrostatic potential variations at the heme edge are depicted in ref. 19, figures 1 and 6.

To determine the integral of the energy transfer rate constant (Eq. 1), the electrostatic potential energy $w(r)$ around all the protein conformers was calculated. At neutral pH it was assumed that all lysines and arginines are protonated, and the aspartic acids, glutamic acids, heme propionate side chains, and carboxyl-terminal acid groups are dissociated (7). Histidines and the acetylated amino terminus are nonprotonated. Partial charges taken from the GROMOS set of charges (22) were assigned to each heavy atom and all hydrogens attached to polar atoms. The protein is represented as an irregularly shaped cavity of low dielectric constant ($\varepsilon = 4$) and zero ionic strength with a total of 1069 fixed embedded charges. The value for the internal dielectric is based on the typical average estimate for protein interiors

(1, 5, 10, 23). Surrounding this cavity is a continuum dielectric with $\varepsilon = 80$, representative of water, with an ionic atmosphere that attenuates the field emanating from the protein charges. The WW-based electrostatic potential field surrounding the protein charge configuration was computed by iterating finite-difference solutions to the linearized Poisson–Boltzmann equation (7). A coarse-grained solution on a cubic lattice (51 × 51 × 51 elements) having a resolution of 4 Å and encompassing a 200 × 200 × 200-Å^3 region centered on the protein was computed for each structure at three ionic strengths. Previously prepared trial solutions based on a simple Coulomb–Debye theory were used to initiate the iterations. Convergence for a single structure at three ionic strengths required a total of 1400 iterations and 42 min of central processing unit (CPU) time on a VAX8800 computer. These grids provide the required potential at large distances from the protein as well as the outer boundary condition for the iteration of a smaller fine-grained 1.0-Å-resolution grid of 61 × 61 × 61 elements. Convergence of each conformer at each ionic strength for the fine-resolution grid required 1000 iterations and an hour of CPU time.

The rate constant (Eq. 1) was evaluated by direct volume integration on a lattice of 1-Å resolution centered on the protein center of mass. Points outside 100 Å made no significant contribution to the integrand and were ignored. Each lattice point was tested against an exclusion grid to determine probe overlaps with the protein; these points did not contribute to the integral. The exclusion grids were determined by embedding each protein conformer on a 67 × 67 × 67-element cubic spatial grid of 1.0-Å resolution. R_{ex}, the exclusion grid parameter, was taken as the terbium chelate donor radius plus the "cube-corner" distance correction of the 1.0-Å-resolution exclusion grid (≈0.7 Å). From considerations of the van der Waals shape of the chelates, R_{ex} was taken as ≈5 Å (13). Test calculations with R_{ex} values of 4.0, 5.0, and 6.0 Å were carried out to assess sensitivity to parameter choice. Full computation of the integral for one protein conformation at one ionic strength at one probe size and for three probe charges required 13 min of computation time on a VAX8800.

Two different methods of specifying the "reaction distance," r_{et}, were tested. The simplest method takes r_{et} to be the distance from the terbium probe center to the heme iron atom. However, since energy transfer most likely takes place over the entire extended π system of the porphyrin, we also took r_{et} as the distance between the donor probe center and the closest of a set of nine porphyrin atoms; the iron atom, the four carbons bridging the pyrrole ring systems, and the four pyrrole nitrogens.

RESULTS AND DISCUSSION

Reaction Criteria. The sensitivity of the energy transfer rate calculations to probe radius, R_{ex}, and reaction-distance criterion, r_{et}, was explored. Calculated values for three values of R_{ex} are compared with experimental in Table 1. As expected from DNA studies (13), the r^6 distance function in Eq. 1 makes the computation sensitive to the choice of R_{ex}. The R_{ex} = 6.0 Å case consistently underestimates the rate because it excludes the donor chelates from the region close to the acceptor region, whereas the R_{ex} = 4.0 Å and 5.0 Å cases give correspondingly higher rates. The intense overall positive electrostatic potential of the protein particularly enhances the sensitivity of the summation for the −1e charged probe.

Calculated rates for the two reaction-distance models, iron atom vs. heme edge, are compared with experiment in Table 2. For an exclusion-grid radius of 5.0 Å, the iron atom-to-probe distance criterion consistently underestimates the energy transfer rate whereas the nine-atom heme edge definition gives good agreement with experiment for all three donor charged states. All subsequent studies reported here use the model parameters (R_{ex} = 5.0 Å and the nine-atom heme shape definition).

Fig. 1 shows the WW electrostatic potential energy map (ionic strength, $I = 0.01$) surrounding a single conformer of the cytochrome *c* protein. The conformation is the 40-psec juncture in the DW simulation. The electric field around cytochrome *c* stabilizes a −1e charge by about 2 units of k_BT in the region of the exposed heme edge. Fig. 1 also shows the spatial region that dominates the energy transfer integrand. There is no significant contribution through the sides or back surface of the protein. The computed rate constant is sensitive almost entirely to the region of space at or near the heme edge/protein solvent dielectric boundary, where the WW method, which accounts for the irregular boundary condition, is expected to give an accurate representation of the potential compared with less rigorous representations of the protein/solvent interface.

MD Effect. Rate constants for the three terbium probes were calculated by the WW method at $I^{1/2}$ = 0.1, 0.2, and 0.3 for 14 unique protein configurations taken from the D80 simulation and 17 from the DW MD simulation. In Fig. 2, the average rate constants are compared with the experimental energy transfer data. Note the overall agreement of the calculations with experiment. The average rates calculated for the conformers from the DW simulation (solid lines) are closer overall to experiment than the D80 simulation results. The agreement with the ionic-strength dependence is strikingly good for both the −1e and the +1e probe cases, the dependence being slightly steeper than experiment for the −1e probe. The average rates calculated from the D80 individual conformer rates are lower than the DW ones for all three probes. This is attributable to the lower steric accessibility of the heme edge in the D80 structures compared with the DW structures as measured by calculations of solvent-accessible surface. A previous study (19) reported that the molecular volumes of the D80 structures are slightly smaller than for DW, indicating a more compact structure in the absence of explicit solvent molecules. The variation of the observed rate constant for the neutral probe at low ionic strength has not been explored, but it could be due to a small

Table 1. Theoretical energy transfer rates for three exclusion-grid distances (R_{ex} = 4.0, 5.0, or 6.0 Å) compared with experimental values

Probe charge	$k \times 10^{-6}$, $M^{-1}sec^{-1}$			
	4.0 Å	5.0 Å	6.0 Å	Exp.
−1e	54.30	21.00	11.04	17.0
0e	6.06	3.35	2.23	4.0
+1e	1.13	0.84	0.67	1.2

Computational results are given for a single protein conformer from the DW set that gave a value closest to the mean theoretical results. Ionic strength, $I = 0.01$.

Table 2. Comparison of the theoretical and experimental rate constant for two methods of defining the reaction distance r_{et}

Probe charge	$k \times 10^{-6}$, $M^{-1}sec^{-1}$		
	Fe-probe criterion	Nine-atom heme shape criterion	Exp.
−1e	5.35	21.00	17.0
0e	1.03	3.35	4.0
+1e	0.34	0.84	1.2

Computational results are given for a single protein conformer from the DW set that gave a value closest to the mean theoretical result. $I = 0.01$.

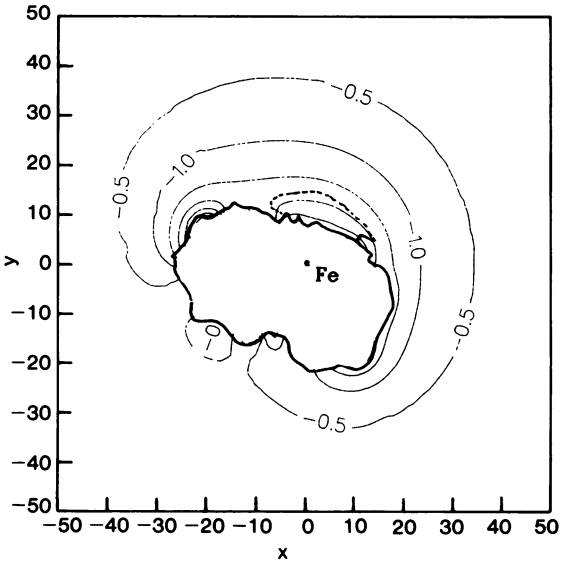

FIG. 1. Electrostatic potential energy contours of a −1e test charge in units of k_BT in the heme plane around horse heart cytochrome *c* in solution of ionic strength, I = 0.01. Values were computed by the WW method with dielectric constant ε = 4 and 80 inside and outside the protein, respectively. Results are for a single conformer coordinate set taken from the DW simulation that gives the closest to the mean theoretical result. The dashed line encloses the region contributing 90% to the theoretical energy transfer rate.

change in average conformation favoring increased heme edge accessibility.

The rms deviations of the calculated average rate constants for both sets of protein conformers are reported in Table 3. Protein side-chain fluctuations in both simulations gave rise to substantial differences in electrostatic potentials and thus in the calculated energy transfer rate constants. For the −1e probe and the DW conformer set, I = 0.01, the highest calculated rate constant was 30 × 10^6 $M^{-1}sec^{-1}$, the average rate was 20.9 × 10^6 $M^{-1}sec^{-1}$, and the lowest was 15 × 10^6 $M^{-1}sec^{-1}$. The high, mean, and low rate-constant spread for the D80 conformer set was even wider under these conditions, being 30 × 10^6, 17.7 × 10^6, and 12 × 10^6 $M^{-1}sec^{-1}$, respectively. This strong dependence on protein conformation underscores the danger of basing predictions on a single protein conformer, such as the crystal structure, where surface side chains are often arbitrarily positioned in the absence of electron density. The rms deviations for the DW simulation are smaller due to retardation of side-chain motion by the explicit water molecules. The simulation (150 psec) was not sufficiently long to allow as complete a sampling of side-chain conformational space in the DW simulation as in the D80. The calculated rates for the initial protein conformation, t = 0, and the conformer that represents the time-average structure from the DW simulation, DW(av), are included in Table 3.

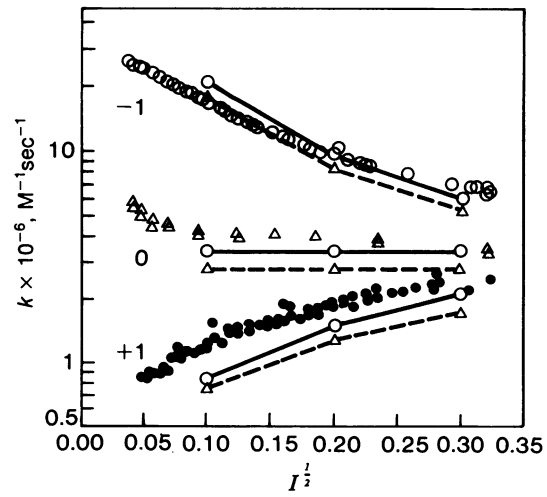

FIG. 2. Ionic-strength dependence of theoretical energy transfer rate constants averaged over the DW (—○—) and D80 (—△—) conformer sets is compared to that of experimental rates (unconnected data points) for three probe charge states, −1e, 0e, and +1e. The rms deviations in the theoretical rate constants arising from rate variations between conformers are shown in Table 3.

Table 3. Energy transfer rate constants for the three probe charge states computed from WW and DH electrostatic potential maps, compared with experimental rates for DW and D80 conformer sets, the starting structure, t = 0, and the ensemble average structure, DW(av)

Probe charge	Structure	$k \times 10^{-6}$, $M^{-1}sec^{-1}$ (rms deviation)		
		I = 0.01	I = 0.04	I = 0.09
		Experimental		
−1e		17.0 (0.3)	9.5 (0.2)	6.8 (0.1)
0e		4.0 (0.1)	3.9 (0.1)	3.6 (0.1)
+1e		1.2 (0.1)	1.95 (0.1)	2.5 (0.1)
		WW method		
−1e	DW*	20.9 (3.8)	9.4 (1.4)	5.9 (0.8)
	D80*	17.7 (5.1)	8.2 (1.7)	5.2 (0.8)
	t = 0	22.0	10.2	6.6
	DW(av)	23.5	10.3	6.2
0e	DW*	3.3 (0.3)	3.3 (0.3)	3.3 (0.3)
	D80*	2.7 (0.3)	2.7 (0.3)	2.7 (0.3)
	t = 0	3.6	3.6	3.6
	DW(av)	3.4	3.4	3.4
+1e	DW*	0.83 (0.08)	1.47 (0.14)	2.10 (0.19)
	D80*	0.75 (0.10)	1.26 (0.17)	1.72 (0.22)
	t = 0	0.87	1.54	2.17
	DW(av)	0.78	1.41	2.05
		DH method		
−1e	DW	13.9 (2.2)	7.4 (1.0)	5.3 (0.7)
	t = 0	16.1	8.5	6.0
	DW(av)	15.0	7.9	5.5
0e	DW	3.3 (0.3)	3.3 (0.3)	3.3 (0.3)
	t = 0	3.6	3.6	3.6
	DW(av)	3.4	3.4	3.4
+1e	DW	1.00 (0.06)	1.74 (0.20)	2.28 (0.18)
	t = 0	1.04	1.75	2.33
	DW(av)	1.02	1.70	2.26

Calculations used probe size R_{cx} = 5.0 Å and nine-atom heme shape definition. Computed and observed rms deviations are in parentheses.
*Data plotted in Fig. 2.

Simple Dielectric Formalism. Rate constants were also determined for electrostatic potential energy maps derived from a simple DH summation for comparison with the rigorous WW procedure described above. The effective dielectric constant for generating the potential maps from the protein charge array was defined as $\varepsilon = \varepsilon_{(H2O)}\, e^{\kappa R_{ij}}$, where κ is the usual DH parameter proportional to the square root of the ionic strength and R_{ij} is the distance of separation between map coordinate and protein charge site. The computed average rates and the rms deviations are given in Table 3 for the set of conformers from the DW trajectory. The predicted average reaction rate for the −1e probe (I = 0.01) is 13.9 × 10^6 $M^{-1}sec^{-1}$ compared to 20.9 × 10^6 $M^{-1}sec^{-1}$ for the WW dielectric treatment. For the +1e probe the DH treatment gave 0.83 × 10^6 $M^{-1}sec^{-1}$ versus 1.0 × 10^6 $M^{-1}sec^{-1}$ for WW. The less rigorous electrostatic treatment predicts smaller electrostatic effects on reaction rates with respect to the neutral probe rate; however, both dielectric treatments agree equally well with the experimental obser-

vations. Additionally, the rms deviations (result of the structural variations between protein conformers) indicate that the effects of structural flexibility on electrostatic effects are as large as the computed differences by these two very different electrostatic algorithms. The calculated rates for the protein starting conformation and the DW time-average structure are included in Table 3.

Conclusions. We have demonstrated that diffusion-enhanced energy transfer studies provide a convenient probe for the electrostatic field surrounding a protein in solution. The comparison of experimental results with two theories of protein electrostatic behavior has allowed us to evaluate the relative accuracy of these methods. The effect of protein side-chain fluctuations was addressed by carrying out electrostatic calculations and rate constant evaluations on sets of structures collected along two MD trajectories of horse heart cytochrome *c*.

The WW procedure for calculating electrostatic maps gave good agreement with experiment and successfully reproduced the ionic-strength dependence of the reaction for all three charge states of the donor probe. Neglecting the protein dielectric properties and treating the entire region outside the protein surface as equivalent to bulk aqueous electrolyte (DH) also gave good agreement with experiment. The calculations were sensitive to the probe radius parameter used in generating the protein excluded volume profile and the definition of the reaction region, indicating that the rate is sensitive to heme accessibility by donor probe. The observed weak salt dependence at low ionic strength of the neutral probe reaction with cytochrome *c* was not explored computationally; however, the effect is similar in magnitude to the computed rate changes for these parameters that affect the apparent heme accessibility (Table 1). As discussed in *Methods*, specific binding of probe to protein at low ionic strength is unlikely, since the luminescence decay was fit to a single exponential.

The intrinsic assumption for all computational studies based on a protein crystal structure is that the x-ray structure adequately represents the time-average solution structure. A substantial body of literature supports this assumption. Exceptions at various levels of structural detail have been clearly identified, however. For example, a salt bridge observed by NMR and chemical studies in solution is absent from the myoglobin crystal structure (24). A further assumption often made is that a calculated quantity derived from analysis of a single average structure is equal to the average calculated for a whole ensemble of thermodynamically accessible structures. Using MD conformers consistent with the x-ray structure, we have shown that the relative merit of electrostatic methods cannot be judged without consideration of protein flexibility. Second, we have calculated an rms deviation for the predicted transfer rates that is attributable to the single-structure assumption. Finally, by considering individual structures in the ensemble and the large variations in the calculated energy transfer rates, we see that transient but possible structures can have properties that are not intrinsic to the average structure. These transient structures may be relevant to stochastic, possibly catalytic events. We conclude that attempts to refine protein computational methods through increased rigor without consideration of all underlying assumptions does not necessarily result in a better method.

This work has been funded at Tennessee Technological University by National Institutes of Health Grants DK01403 and GM34248 and by the donors of the Petroleum Research Fund as administered by the American Chemical Society and at the University of California, Davis, by National Institutes of Health Grant GM25909. S.H.N. is a recipient of a National Institutes of Health Research Career Development Award.

1. Matthew, J. B. (1985) *Annu. Rev. Biophys. Chem.* **14,** 387–417.
2. Rush, J. D. & Koppenol, W. H. (1985) *Biochim. Biophys. Acta* **936,** 187–192.
3. Northrup, S. H., Reynolds, J. C. L., Miller, C. M., Forrest, K. J. & Boles, J. O. (1986) *J. Am. Chem. Soc.* **108,** 8162–8170.
4. Allison, S. A., Ganti, G. & McCammon, J. A. (1985) *Biopolymers* **24,** 1323–1336.
5. Gilson, M. K. & Honig, B. H. (1988) *Nature (London)* **330,** 84–86.
6. Allison, S. A., Bacquet, R. J. & McCammon, J. A. (1988) *Biopolymers* **27,** 251–269.
7. Northrup, S. H., Boles, J. O. & Reynolds, J. C. L. (1987) *J. Phys. Chem.* **91,** 5991–5998.
8. Northrup, S. H., Luton, J. A., Boles, J. O. & Reynolds, J. C. L. (1987) *J. Comp. Aided Molec. Design* **1,** 291–311.
9. Northrup, S. H., Boles, J. O. & Reynolds, J. C. L. (1988) *Science* **241,** 67–70.
10. Warshel, A. & Russell, S. T. (1984) *Q. Rev. Biophys.* **17,** 283–422.
11. Warwicker, J. & Watson, H. C. (1982) *J. Mol. Biol.* **157,** 671–679.
12. Gilson, M. K. & Honig, B. H. (1988) *Proteins* **3,** 32–52.
13. Wensel, T. G., Meares, C. F., Vlachy, V. & Matthew, J. B. (1986) *Proc. Natl. Acad. Sci. USA* **83,** 3267–3271.
14. Wensel, T. G. (1985) Ph.D. dissertation (Univ. of California, Davis).
15. Stryer, L., Thomas, D. D. & Meares, C. F. (1982) *Annu. Rev. Biophys. Bioeng.* **11,** 203–213.
16. Forster, T. (1948) *Ann. Phys. (Leipzig)* **2,** 55–75.
17. Brautigan, D. L., Ferguson-Miller, S. & Margoliash, E. (1978) *Methods Enzymol.* **53,** 128–137.
18. Chen, P. S., Jr., Toribara, T. Y. & Warner, H. (1956) *Anal. Chem.* **28,** 1756–1760.
19. Wendoloski, J. J. & Matthew, J. B. (1989) *Proteins* **4,** 313–321.
20. Brooks, B. R. (1987) *Supercomputing Research in Chemistry and Chemical Engineering* (Am. Chem. Soc., Washington), pp. 123–145.
21. Jorgensen, W. L., Chandrasekhar, J., Madura, J., Impey, R. W. & Klein, M. L. (1983) *J. Chem. Phys.* **79,** 926–935.
22. Berendsen, H. J. C., Postma, J. P. M., van Gunsteren, W. F. & Hermans, J. (1981) in *Intermolecular Forces*, ed. Pullman, B. (Reidel, Dordrecht), pp. 331–350.
23. Pethig, R. (1979) *Dielectric and Electronic Properties of Biological Materials* (Wiley, Chichester, U.K.).
24. Botelho, L. H., Friend, S. H., Matthew, J. B., Lehman, L. D., Hanania, G. I. H. & Gurd, F. R. N. (1978) *Biochemistry* **17,** 5197–5205.